



7N-05
197747
348

TECHNICAL NOTE

D-215

VERTICAL-TAIL LOADS MEASURED IN FLIGHT ON FOUR AIRPLANE
CONFIGURATIONS AT TRANSONIC AND SUPERSONIC SPEEDS

By Robert D. Reed

Flight Research Center
Edwards, Calif.

NATIONAL AERONAUTICS AND SPACE ADMINISTRATION
WASHINGTON

February 1960

(NASA-TN-D-215) VERTICAL-TAIL LOADS
MEASURED IN FLIGHT ON FOUR AIRPLANE
CONFIGURATIONS AT TRANSONIC AND SUPERSONIC
SPEEDS (NASA, Flight Research Center) 34 p

N89-70902

Unclas
00/05 0197747

NATIONAL AERONAUTICS AND SPACE ADMINISTRATION

TECHNICAL NOTE D-215

VERTICAL-TAIL LOADS MEASURED IN FLIGHT ON FOUR AIRPLANE

CONFIGURATIONS AT TRANSONIC AND SUPERSONIC SPEEDS

By Robert D. Reed

SUMMARY

Aerodynamic loads were obtained for the vertical tails of four airplane configurations: the X-5, an F-100 with a small vertical tail, an F-100 with a large vertical tail, and the X-1E. Effects of sideslip angle, rudder deflection, and Mach number on the vertical-tail loads are presented, together with the spanwise centers of pressure, for trim flight at altitudes from 40,000 feet to 70,000 feet and at Mach numbers from 0.70 to 2.08. Also shown is the directional stability for each configuration as calculated by use of vertical-tail loads.

Currently available methods for estimating load due to sideslip are adequate for subsonic and supersonic speeds. The results obtained from methods for estimating load due to rudder deflection show good agreement with flight data at subsonic speeds. Estimations of spanwise centers of pressure due to sideslip showed fair to good agreement with flight data, depending on the configuration, and good agreement was shown for spanwise centers of pressure due to rudder deflection at subsonic speeds.

Good agreement with results from accepted methods for calculating total airplane directional stability from flight data was obtained by using measurements of vertical-tail loads when corrections for aileron yawing moment and rudder-carryover effects were included.

INTRODUCTION

Several papers published during the past few years have made available the results of investigations applicable to the prediction of vertical-tail loads (refs. 1 to 8). In these investigations, studies were made of the effects of such configuration factors as the location of the horizontal tail and the size and shape of the fuselage in the vicinity of the vertical tail (refs. 1 and 2). Although results of these studies have been substantiated to a considerable extent at subsonic speeds by full-scale flight data, published flight data in the transonic and the supersonic speed ranges are relatively scarce. This

paper, therefore, presents a summary of vertical-tail loads measured during research flights with the X-5 airplane, an F-100 airplane with a small vertical tail, an F-100 with a large vertical tail, and the X-1E airplane. The flights were conducted at the NASA Flight Research Center, Edwards, Calif. Test ranges varied in Mach number from the lowest speed of $M = 0.70$ for the X-5 airplane to the highest speed of $M = 2.08$ for the X-1E. Data for all airplanes were obtained at relatively small angles of attack (trim flight) and sideslip. Comparisons are made with the loads estimated by using currently available methods.

SYMBOLS

b	tail-panel span, ft
b_w	wing span, ft
C_b	tail-panel aerodynamic bending-moment coefficient, positive bending moment for side force to right, $\frac{\text{Root bending moment}}{qSb}$
C_n	yawing-moment coefficient, airplane nose right positive, $\frac{\text{Yawing moment}}{qS_w b_w}$
$C_{n\beta}$	variation of yawing-moment coefficient with sideslip angle, $\partial C_n / \partial \beta$, per deg
C_Y	tail-panel aerodynamic side-force coefficient, positive side force right, $\frac{\text{Side force}}{qS}$
$C_{Y\beta}$	variation of side-force coefficient with sideslip angle, $\partial C_Y / \partial \beta$, per deg
$C_{Y\delta_r}$	variation of side-force coefficient with rudder deflection, $\partial C_Y / \partial \delta_r$, per deg
c	tail-panel chord, ft
c_p	tail-panel spanwise center of pressure, percent span from root
M	Mach number

p	rolling velocity, radians/sec
q	dynamic pressure, lb/sq ft
r	yawing velocity, radians/sec
S	tail-panel area, sq ft
S_w	wing area, sq ft
t	time, sec
β	angle of sideslip at tail panel, positive sideslip right, deg
β_A	airplane angle of sideslip, deg
δ_{at}	total aileron deflection, deg
δ_r	rudder deflection, positive when trailing edge left, deg

AIRPLANE CONFIGURATIONS

The four airplanes considered in this paper are the X-5, hereafter referred to as configuration A; an F-100 with a small vertical tail, configuration B; an F-100 with a large vertical tail, configuration C; and the X-1E, configuration D.

Photographs of the test airplanes are shown in figure 1, and three-view drawings are shown in figure 2. Side views of the four vertical tails, defining the tail panels over which the loads were measured, are presented in figure 3. Table I gives the physical dimensions of the tail panels and rudders.

Configuration A

For these tests the wing of the X-5 variable-sweep airplane was swept back 60° . The wing is located at a high midwing position on the fuselage. The rear portion of the fuselage on which the vertical tail is mounted is relatively small, with a diameter about 30 percent of the vertical-tail-panel span. The horizontal tail is mounted midheight on the fuselage with the engine exhausting beneath the tail boom.

Configuration B

The F-100 airplane has a low wing which is swept back 45° and a low horizontal tail swept back 45° . A dorsal fin covers the inboard 40 percent of the leading edge of the vertical-tail panel. An inboard rudder covers approximately 55 percent of the panel span and has a relatively large gap of $1/2$ inch (varies from 0.005-local chord to 0.009-local chord). An overhang, about 9.3 percent of the root chord, exists near the trailing edge of the vertical-tail panel (fig. 3). The fuselage in the vicinity of the vertical-tail panel has a diameter about 75 percent of the panel span, thus the horizontal tail is 75 percent of the panel span below the panel root chord.

H
1
4
0

Configuration C

This configuration has the same general characteristics as configuration B, except that the leading edge of the vertical tail is extended forward and the tip extended outward so that the area is increased by 27 percent, with corresponding changes to the aspect ratio and taper ratio. In this configuration the dorsal fin covers the inboard 28 percent of the leading edge, the rudder extends to about 42 percent of the panel span, and the fuselage diameter is about 60 percent of the panel span.

Configuration D

The X-1E rocket research airplane has an unswept wing mounted mid-height on the fuselage. An unswept horizontal tail is mounted on the vertical tail a considerable distance above the fuselage. A dorsal fin leads into the lower portion of the vertical tail, but does not extend above the base of the instrumented panel; thus the leading edge of the panel is exposed to the airstream. The fuselage diameter in the vicinity of the vertical-tail panel is about 55 percent of the panel span. The tail-panel root chord is located above the fuselage a distance equal to 52 percent of the panel span. The vertical-tail panel as defined for this investigation consists of only about 50 percent of the total exposed surface area of the vertical tail and dorsal fin. About 44 percent of the rudder extends inboard from the tail panel.

INSTRUMENTATION AND ACCURACY

Standard NASA recording instruments were used to measure the quantities pertinent to this investigation. Strain gages were installed on the internal structure and skin of the vertical tails at the locations

shown in figure 3. The strain-gage installations were calibrated for shear and bending moment by using the calibration procedure outlined in reference 9. Sideslip angle was measured by a vane mounted on a boom extending forward of the nose of each test airplane, thus a correction for effects of yawing velocity during oscillation maneuvers was made to obtain true angle of sideslip at the tail panel.

Estimated accuracies of the quantities used in this investigation are:

Mach number	±0.02 subsonic
	±0.01 supersonic
Angle of sideslip, deg	±0.5 absolute
	±0.1 incremental
Angular velocities (pitching, rolling, yawing), radians/sec	±0.01
Control positions, deg	±0.25 absolute
	±0.10 incremental
Measured shear, lb	±100
Measured bending moment, in-lb	±1,000

TESTS

The data presented in this paper were obtained from rudder pulses at zero sideslip followed by controls-fixed oscillations and from gradually increasing wings-level sideslips. Both types of maneuvers were executed in trim flight.

In the rudder-pulse and oscillation maneuver the airplanes were trimmed for level flight at zero sideslip angle, at which time the rudder was pulsed. The rudder was then held in neutral position while the airplane oscillated in sideslip.

In the wings-level sideslip maneuver, the rudder deflection was increased gradually so that a balanced condition existed between the aerodynamic yawing moment of the wing-fuselage and the aerodynamic moment produced by the load on the vertical tail. In most instances, to hold the wings level, ailerons were deflected to restrain the airplane from rolling.

The test ranges covered were:

Configuration	Mach number	Altitude, ft	Reynolds number, $R \times 10^{-6}$, per ft
A	0.70 to 0.91	40,000	1.4 to 1.8
B	.78 to 1.30	40,000	1.5 to 2.5
C	.79 to 1.17	40,000	1.5 to 2.3
D	.81 to 2.08	50,000 to 70,000	.6 to 9.5

RESULTS AND DISCUSSION

The vertical-tail-loads data presented in this paper are discussed in the following order: the effects of sideslip and rudder deflection on the vertical-tail loads, the effects of sideslip and rudder deflection on the spanwise centers of pressure, and the contributions of the vertical-tail loads to the overall airplane directional stability. The data presented were corrected for inertias of the tails and are, therefore, the aerodynamic loads. For configurations B and C (fig. 3) the dorsal-fin structure was such that the major portion of the dorsal-fin loads was carried over to the fuselage, hence the loads were not considered to be part of the test panels. For configuration D the test panel was calibrated to exclude the effects of load from the portion of the rudder inboard of the panel.

Vertical-Tail Load

Effects of sideslip.- The effects of sideslip on the panel loads were determined from data obtained during oscillations in sideslip with all controls held fixed. Presented in figure 4 is a representative time history of a rudder-pulse and oscillation maneuver performed at a Mach number of 0.89 with configuration C. Presented are rudder deflection, airplane sideslip angle, panel side-force and bending-moment coefficients, and yawing and rolling angular velocities. The tail-panel lift-curve slope obtained from the time history of figure 4 is shown in figure 5.

The lift-curve slopes obtained from figure 5 and similar measured data from all four configurations are presented in figure 6 as the variation of $C_{Y\beta}$ with Mach number. Also shown are lift-curve slopes estimated by using the following procedure: The lift-curve slope for an isolated panel was found from charts of reference 3 for subsonic speeds and from charts of reference 4 for supersonic speeds. Effects of fuselage

and horizontal tail on the lift-curve slopes were determined by using charts from reference 2. Because of the unusual fuselage of configuration A, it was considered necessary to include the effects of the engine exhaust. The effective side projection of the tail boom was assumed to be twice the actual size of the boom as a result of the engine wake behind the underslung engine.

As can be seen in figure 6, the estimated lift-curve slopes show adequate agreement with the flight results at subsonic and supersonic speeds.

Effects of rudder.- The effects of rudder on the vertical-tail-panel loads were determined from the first part of the rudder pulses during which the airplane remained in a steady-state condition for a limited time (fig. 4). Since no airplane motion was involved, the loads induced upon the tail panel from this phase of the rudder pulse were due entirely to rudder deflection. An example of the contribution of the rudder to the load on the vertical tail, obtained from the time history of figure 4, is shown in figure 7.

Values of $C_{Y\delta_r}$ obtained from figure 7 and similar measured data for all four configurations are shown in figure 8 as a function of Mach number. The rudder effectiveness is comparatively constant up to $M = 0.9$ and exhibits a typical decrease with increasing Mach number for all four configurations.

Estimates of rudder effectiveness at subsonic speeds for comparison with flight data are also shown. To estimate rudder effectiveness, charts presenting lifting effectiveness of inboard flaps were used from references 5 and 6. Because of the relatively large unsealed rudder gap on configurations B and C, a correction of -0.0009 in $C_{Y\delta_r}$ for configuration B and -0.0007 for configuration C was made, based on charts of reference 7. As can be seen in figure 8, the results from this method for estimating the rudder effectiveness for subsonic speeds show good agreement with flight data.

Center of Pressure

Effects of sideslip.- The spanwise center of pressure experienced on the panel during a controls-fixed oscillation was obtained by plotting the panel bending-moment coefficient against the panel normal-force coefficient and measuring the slope. An example of C_b plotted against C_y , taken from figure 4, is shown in figure 9. This slope is shown in figure 10 as c_p plotted against M for the four configurations. Figure 10 shows no discernible variation of center of pressure with Mach number for the four configurations throughout the test Mach number ranges.

Also shown in figure 10 are estimated centers of pressure from the charts of reference 3 for subsonic speeds and from reference 8 for supersonic speeds. The agreement between the measured centers of pressure and those estimated by these simplified methods is good for configurations A and D but only fair for configurations B and C. The largest discrepancy is approximately 10-percent span, with the measured values outboard of the estimated centers of pressure.

Effects of rudder.- Figure 11, obtained from figure 4, presents an example of the variation of C_b with C_y from which the spanwise centers of pressure during rapid rudder inputs were obtained. The centers of pressure obtained in this manner are presented in figure 12 as c_p plotted against M for the four configurations. In figure 12 no variation of c_p with M is discernible for any of the four configurations.

Also shown in figure 12 are estimated centers of pressure taken from charts of references 5 and 6. Values obtained by this method of estimating centers of pressure due to rudder deflection show good agreement with flight data for all four configurations.

Directional Stability

The total directional stability of each of the four airplane configurations was determined by using vertical-tail loads measured during controls-fixed oscillations and also during steady-sideslip maneuvers. To accomplish this, the contributions of the tail panel and the wing-fuselage to the total airplane directional stability were determined.

The contributions of the tail panels to the directional stability were determined by converting the loads measured on the vertical-tail panels during oscillation maneuvers (fig. 6) to yawing moments about the center of gravity of the airplane.

The contributions of the wing-fuselage to the directional stability were determined from the loads measured on the vertical-tail panels during steady-sideslip maneuvers, in which the wing-fuselage yawing moment (ailerons deflected) was balanced by the yawing moment produced by the vertical-tail loads (rudder deflected). A time history of a typical steady-sideslip maneuver is presented in figure 13 showing rudder deflection, airplane angle of sideslip, aileron position, panel side-force and bending-moment coefficients, and yawing and rolling angular velocities. Figure 14 is an example of C_y plotted against β obtained during the steady-sideslip maneuvers of figure 13. Values of C_y/β obtained from figure 14 and similar measured data for all four configurations are shown in figure 15 as a function of Mach number.

To obtain the yawing moment of the wing fuselage (in the presence of the vertical tail) with no control deflections, it was necessary to convert the data of figure 15 to yawing moment, then to correct for the yawing moment due to aileron deflection and yawing moment due to rudder-carryover effects (rudder-induced loads on vertical-tail and fuselage surfaces inboard of strain-gage-reference station). The latter correction was necessary primarily for configuration D (fig. 3). The corrections for yawing moment due to aileron deflection were obtained from reference 10 for configurations B and C and from unpublished flight data for configuration D. Corrections for rudder-carryover effects were obtained by taking the difference between the total yawing moment due to rudder deflection and the yawing moment resulting from rudder deflection as measured by panel loads ($C_{Y\delta_r}$ from fig. 8). The total yawing moment due to rudder deflection was obtained from flight data of reference 10 for configurations B and C and from unpublished flight data for configuration D. Because of the unavailability of necessary data, corrections for aileron yawing moment and rudder-carryover effects were not made for configuration A.

A breakdown of the tail-panel and wing-fuselage contributions to directional stability for the four configurations is shown in figure 16. The tail-panel contribution is the converted data of figure 6, and the wing-fuselage contribution is the converted data of figure 15 corrected for aileron and rudder-carryover effects. The positive wing-fuselage yawing moment for configuration D results from the fact that the moment from the vertical tail inboard of the test panel is included with the wing-fuselage yawing moment. The total airplane directional stability, obtained by adding the vertical-tail-panel contribution to the wing-fuselage contribution, is shown in figure 16.

Also shown in figure 16 is the yawing-moment coefficient of the total airplane for configuration A taken from unpublished wind-tunnel data from the Langley high-speed 7- by 10-foot wind tunnel, for configurations B and C from flight data of reference 11, and for configuration D from unpublished flight data. When corrections for aileron yawing-moment and rudder-carryover effects are applied to loads measurements for configurations B, C, and D, the total airplane directional stability obtained agrees well with that obtained by other methods. There is, however, considerable disagreement between the uncorrected data for configuration A and those obtained by wind-tunnel data, with the flight values being about half the wind-tunnel values. The disagreement is believed to result from a large yawing moment caused by large aileron deflection (fig. 13), for which a correction was not available.

CONCLUDING REMARKS

Vertical-tail loads measured on four airplane configurations for trim flight at altitudes from 40,000 feet to 70,000 feet and at Mach numbers from 0.70 to 2.08 are presented. Shown are the effects of Mach number, sideslip, and rudder deflection at low angles of attack and sideslip.

Currently available methods for estimating load due to sideslip were adequate for subsonic and supersonic speeds. The results from methods of estimating load due to rudder deflection showed good agreement with flight data at subsonic speeds. Estimations of spanwise centers of pressure due to sideslip showed fair to good agreement with flight data, depending on the configuration, and good agreement was shown for spanwise center of pressure due to rudder deflection at subsonic speeds.

Good agreement with results from accepted methods for calculating total airplane directional stability from flight data was obtained by using measurements of vertical-tail loads when corrections for aileron yawing-moment and rudder-carryover effects were included.

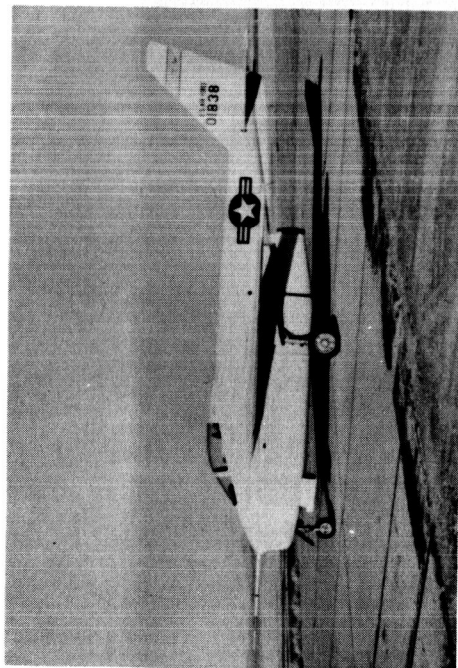
Flight Research Center,
National Aeronautics and Space Administration,
Edwards, Calif., October 23, 1959.

REFERENCES

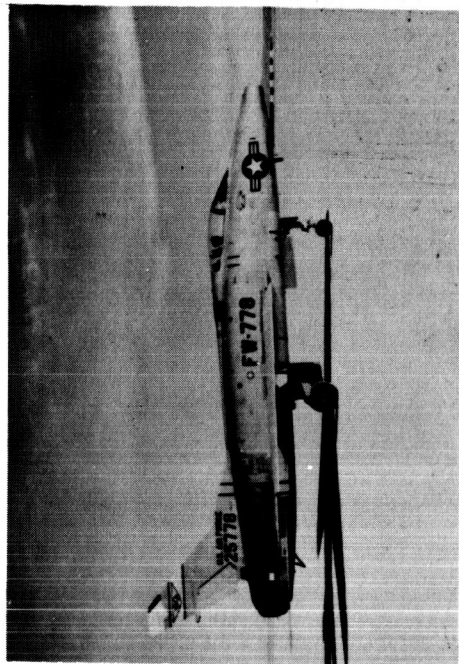
1. Brewer, Jack D., and Lichtenstein, Jacob H.: Effect of Horizontal Tail on Low-Speed Static Lateral Stability Characteristics of a Model Having 45° Sweptback Wing and Tail Surfaces. NACA TN 2010, 1950.
2. Goodwin, Frederick K., and Kaattari, George E.: Estimation of Directional Stability Derivatives at Small Angles and Subsonic and Supersonic Speeds. NASA MEMO 12-2-58A, 1958.
3. DeYoung, John, and Harper, Charles W.: Theoretical Symmetric Span Loading at Subsonic Speeds for Wings Having Arbitrary Plan Form. NACA Rep. 921, 1948.
4. Martin, John C., and Malvestuto, Frank S., Jr.: Theoretical Force and Moments Due to Sideslip of a Number of Vertical Tail Configurations at Supersonic Speeds. NACA TN 2412, 1951.
5. Diederich, Franklin W., and Zlotnick, Martin: Calculated Spanwise Lift Distributions, Influence Functions, and Influence Coefficients for Unswept Wings in Subsonic Flow. NACA Rep. 1228, 1955.
6. Diederich, Franklin W., and Zlotnick, Martin: Calculated Spanwise Lift Distributions and Aerodynamic Influence Coefficients for Swept Wings in Subsonic Flow. NACA TN 3476, 1955.
7. Lyons, D. J., and Bisgood, P. L.: An Analysis of the Lift Slope of Aerofoils of Small Aspect Ratio, Including Fins, With Design Charts for Aerofoils and Control Surfaces. R. & M. No. 2308, British A.R.C., 1950.
8. Martin, John C., and Jeffreys, Isabella: Span Load Distributions Resulting From Angle of Attack, Rolling, and Pitching for Tapered Sweptback Wings With Streamwise Tips. Supersonic Leading and Trailing Edges. NACA TN 2643, 1952.
9. Skopinski, T. H., Aiken, William S., Jr., and Huston, Wilber B.: Calibration of Strain-Gage Installations in Aircraft Structures for the Measurement of Flight Loads. NACA Rep. 1178, 1954.
10. Matranga, Gene J., and Peele, James R.: Flight-Determined Static Lateral Stability and Control Characteristics of a Swept-Wing Fighter Airplane to a Mach Number of 1.39. NACA RM H57A16, 1957.
11. Drake, Hubert M., Finch, Thomas W., and Peele, James R.: Flight Measurements of Directional Stability to a Mach Number of 1.48 for an Airplane Tested With Three Different Vertical Tail Configurations. NACA RM H55G26, 1955.

TABLE I.- PHYSICAL CHARACTERISTICS OF TAIL PANELS AND RUDDERS

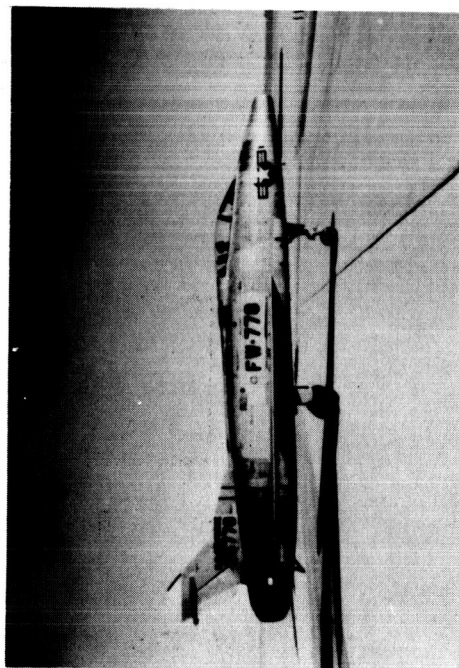
	Configuration			
	A	B	C	D
Panel:				
Area, sq ft	19.3	33.3	42.5	14.9
Span, in.	61.9	73.1	95.0	53.6
Aspect ratio	1.38	1.11	1.48	1.34
Sweep at 25-percent chord, deg	41	45	45	15.5
Taper ratio	0.34	0.44	0.30	0.50
Rudder:				
Area, sq ft	4.68	7.86	7.86	2.87
Span, in.	55.1	40.0	40.0	47
Sweep of leading edge, deg	26	40	40	0



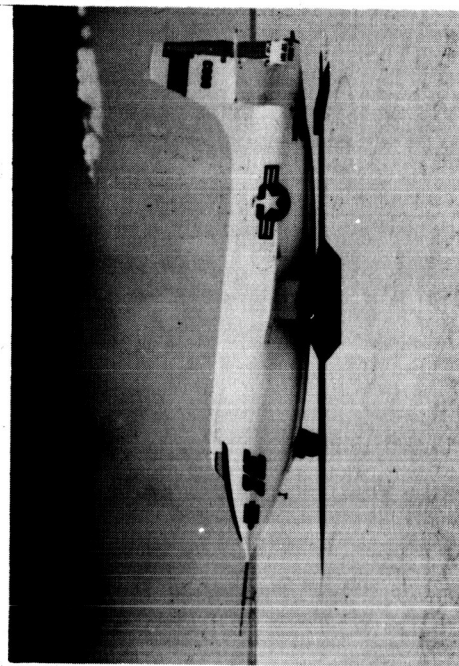
X-5 (Configuration A)



F-100 (Configuration C)



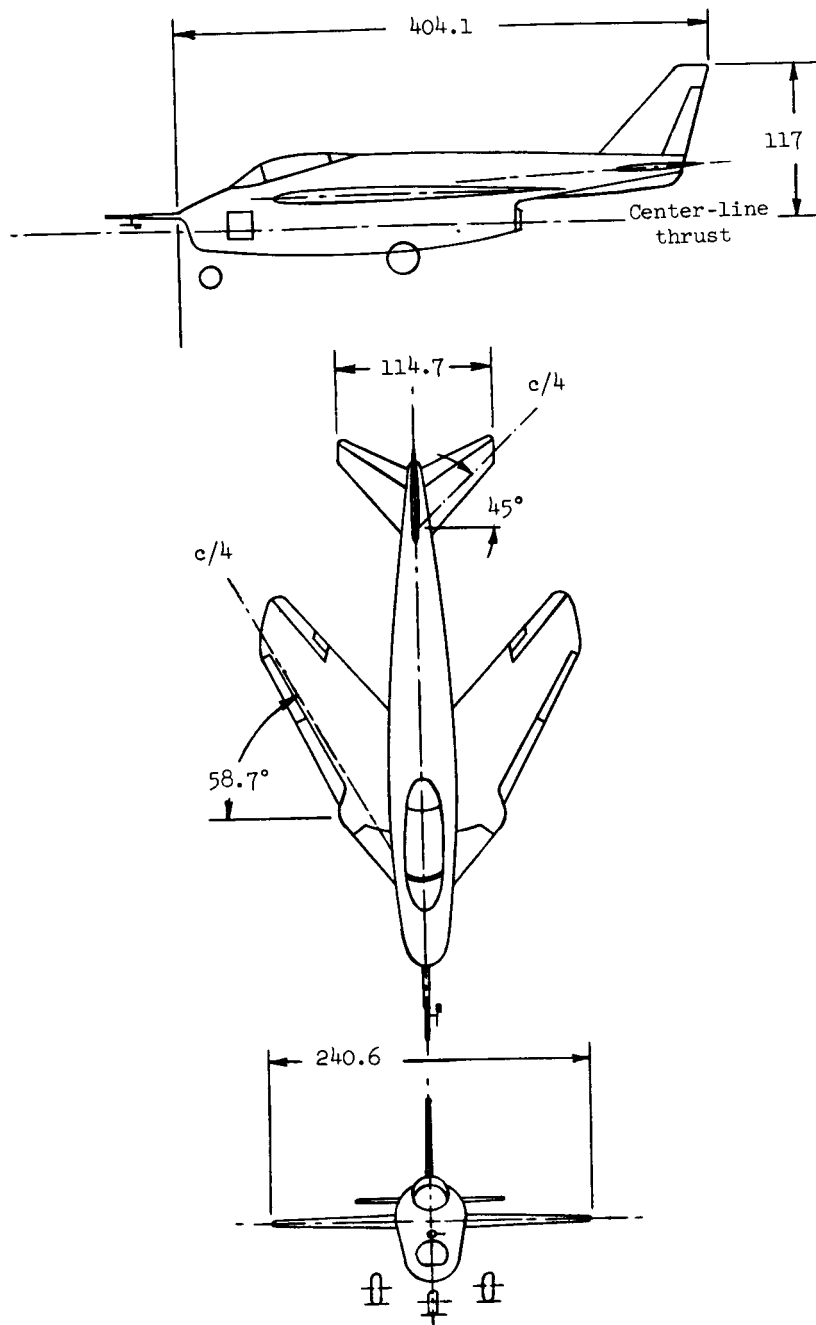
F-100 (Configuration B)



X-1E (Configuration D)

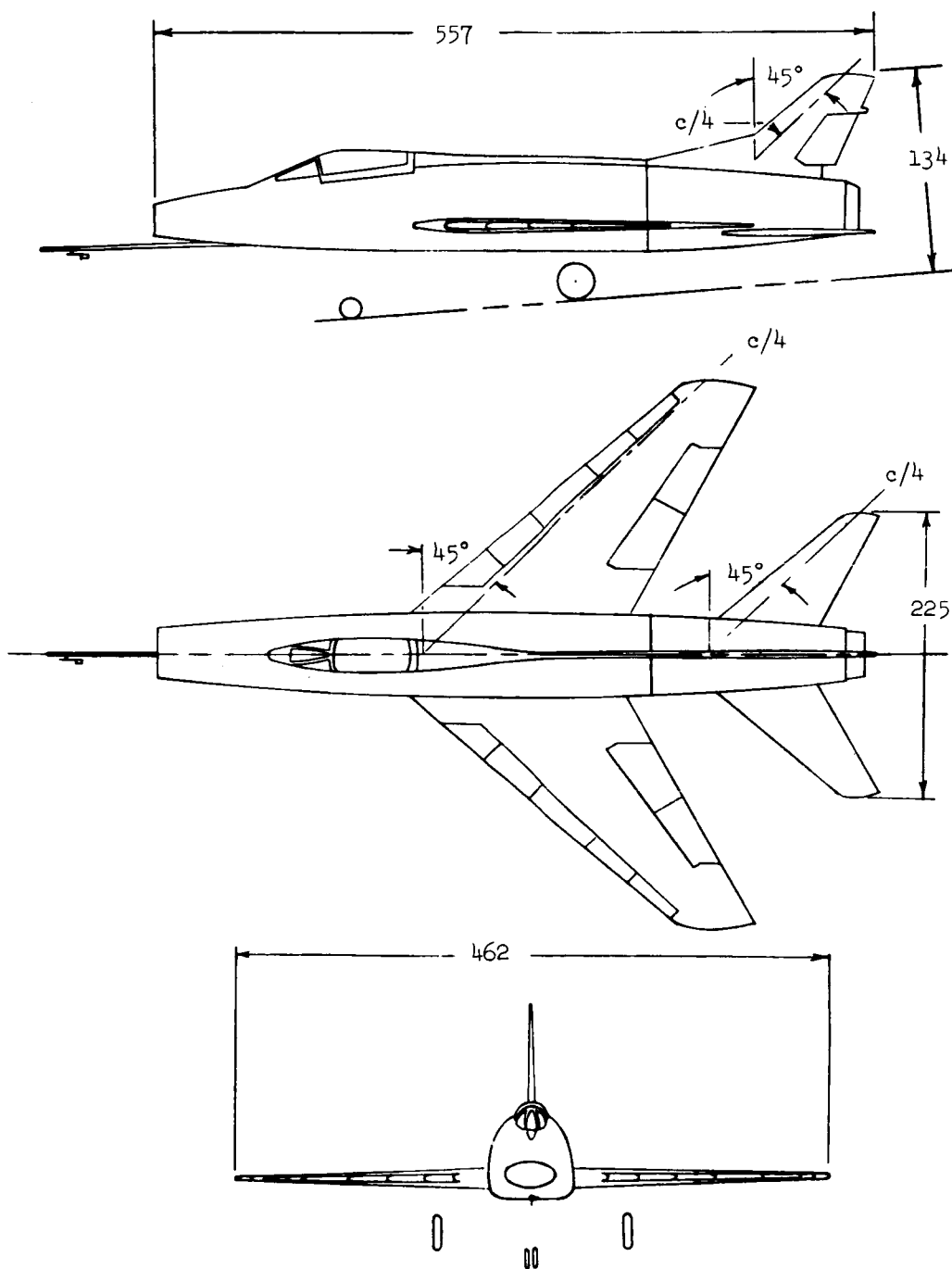
Figure 1.- Photographs of the test airplanes.

E-59-0-0-393



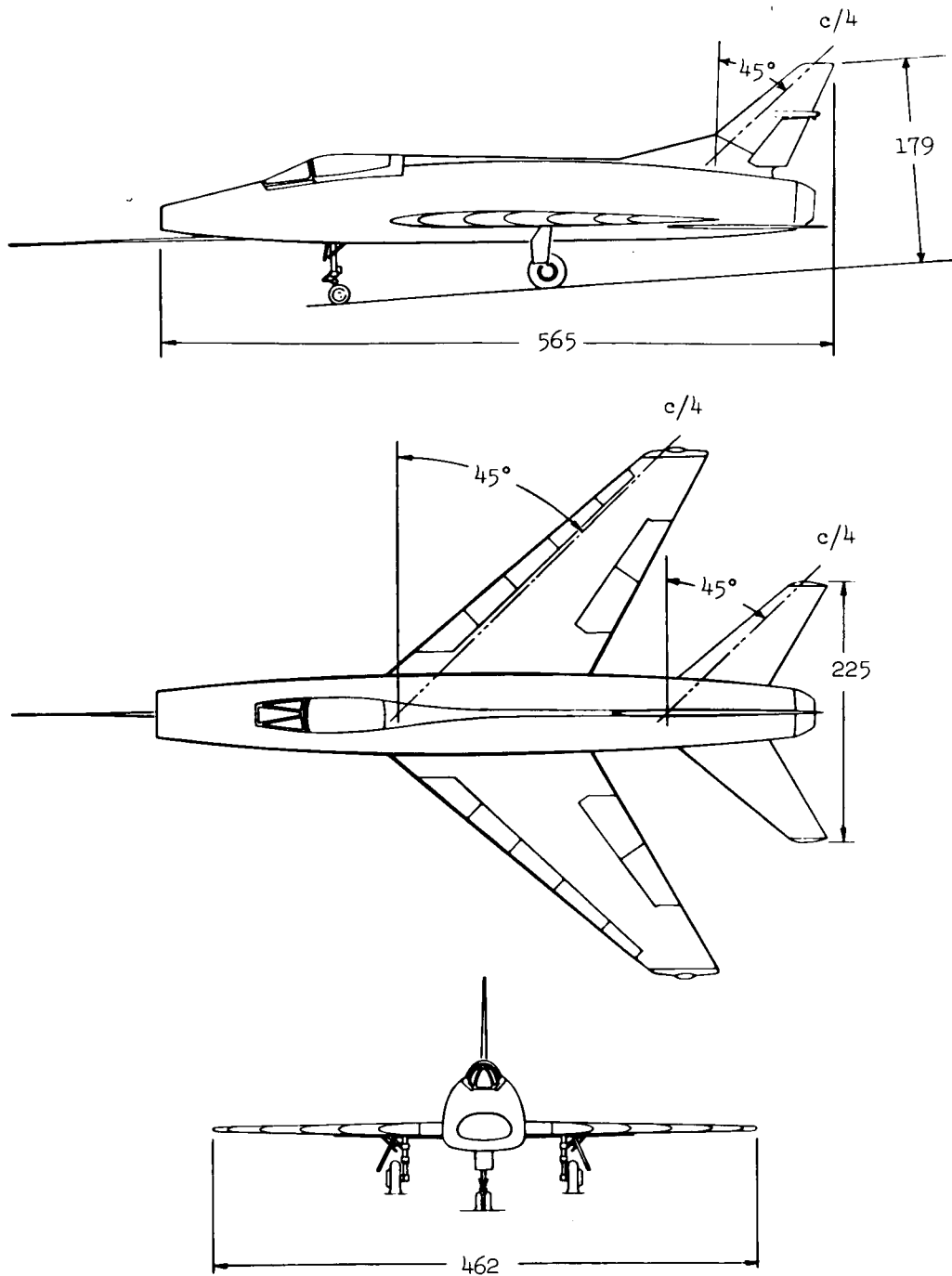
(a) X-5 (configuration A).

Figure 2.- Three-view drawings of the test airplanes. All dimensions in inches unless otherwise noted.



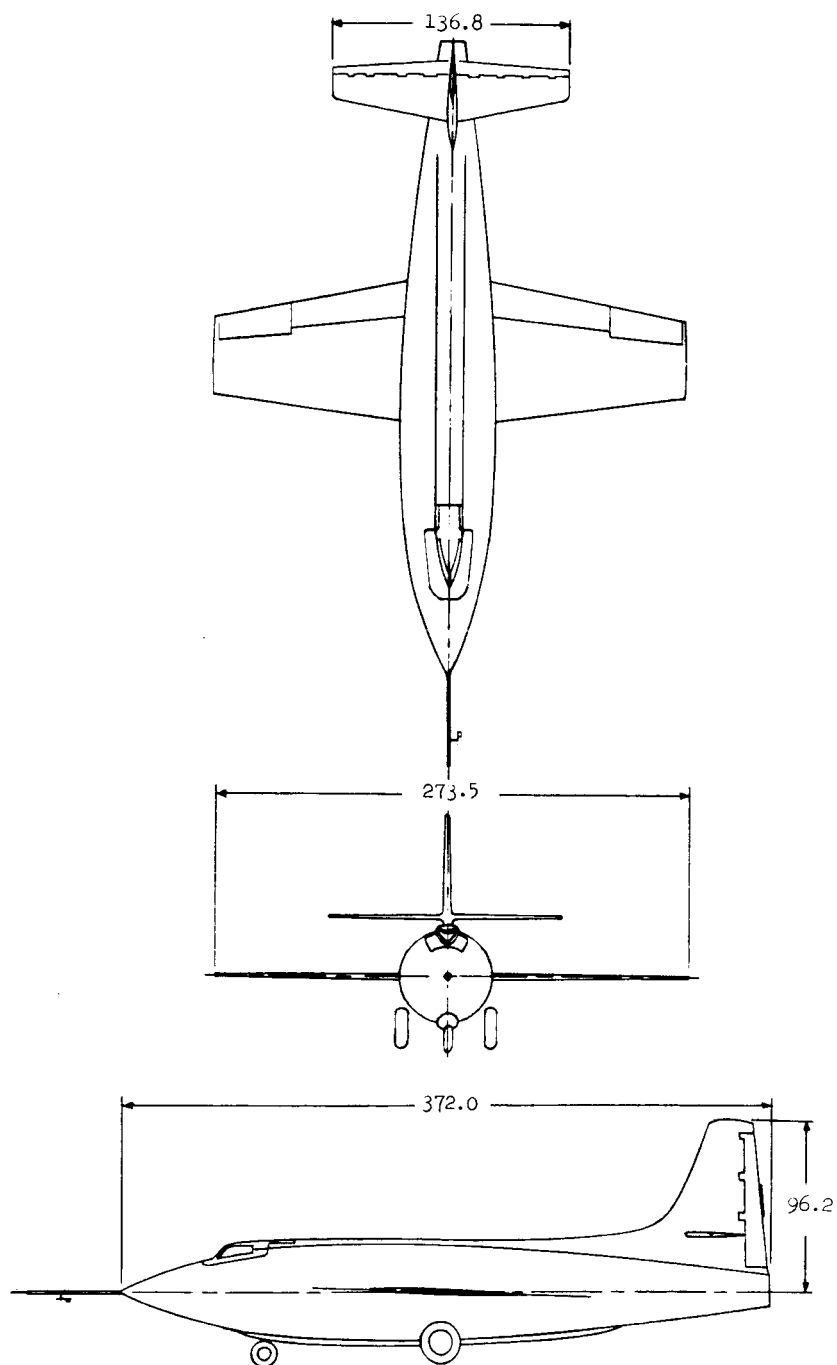
(b) F-100 (configuration B).

Figure 2.- Continued.



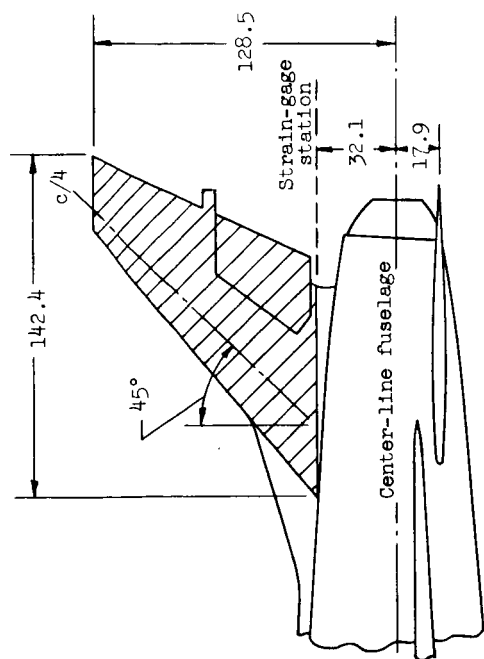
(c) F-100 (configuration C).

Figure 2.- Continued.

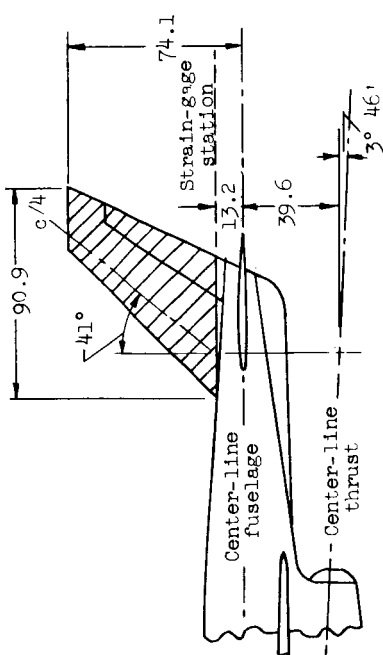


(d) X-1E (configuration D).

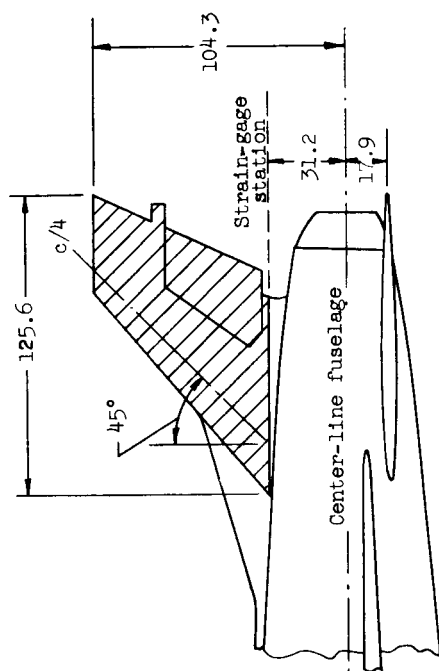
Figure 2.- Concluded.



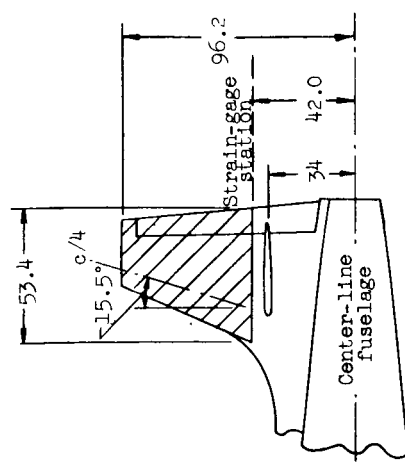
CONFIGURATION C



CONFIGURATION A



CONFIGURATION B



CONFIGURATION D

Figure 3.- Side-view drawings of the four vertical-tail configurations with test panels indicated by crosshatching. All dimensions in inches unless otherwise noted.

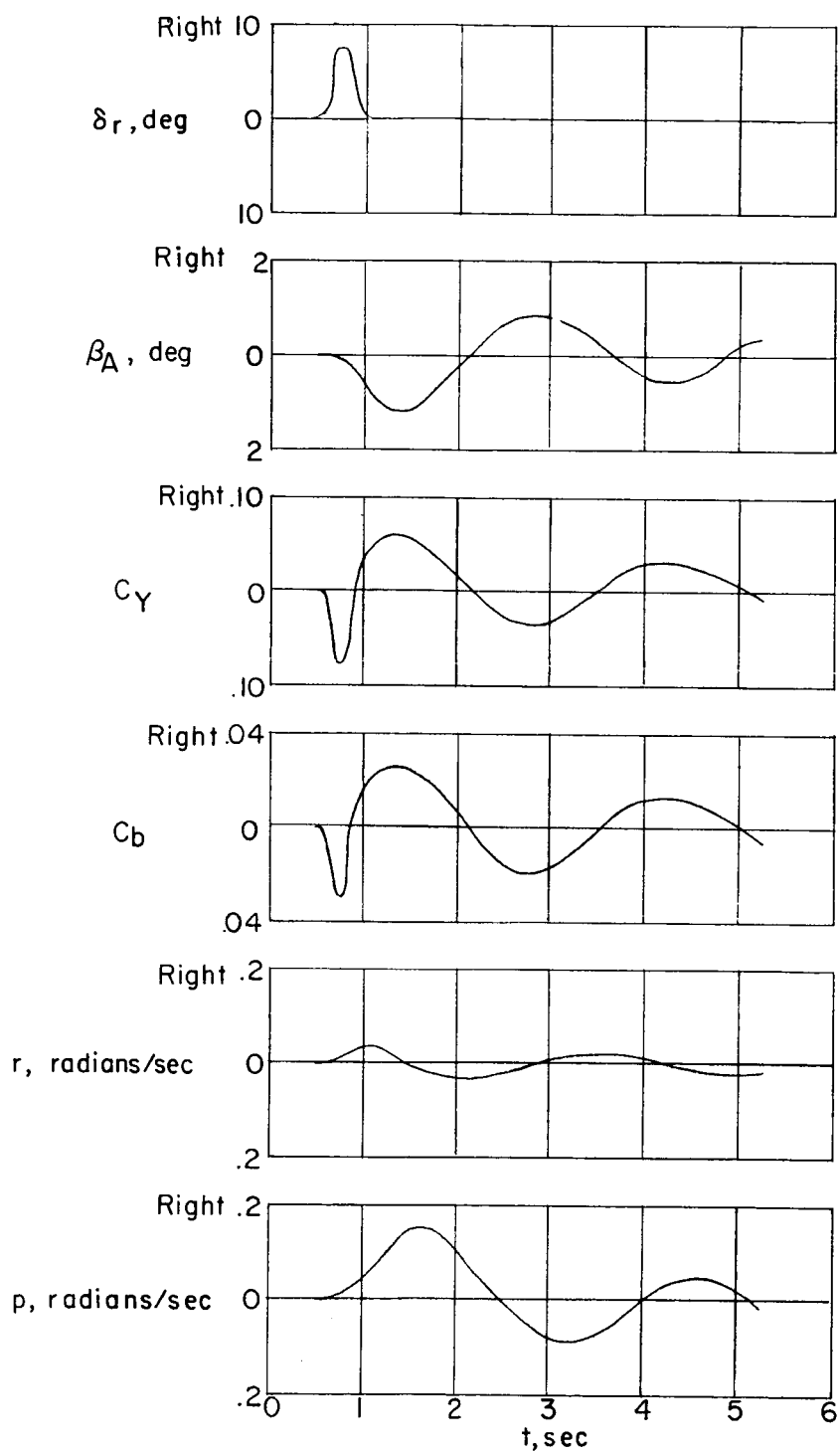


Figure 4.- Time history of a typical rudder-pulse and oscillation maneuver. Configuration C; $M = 0.89$.

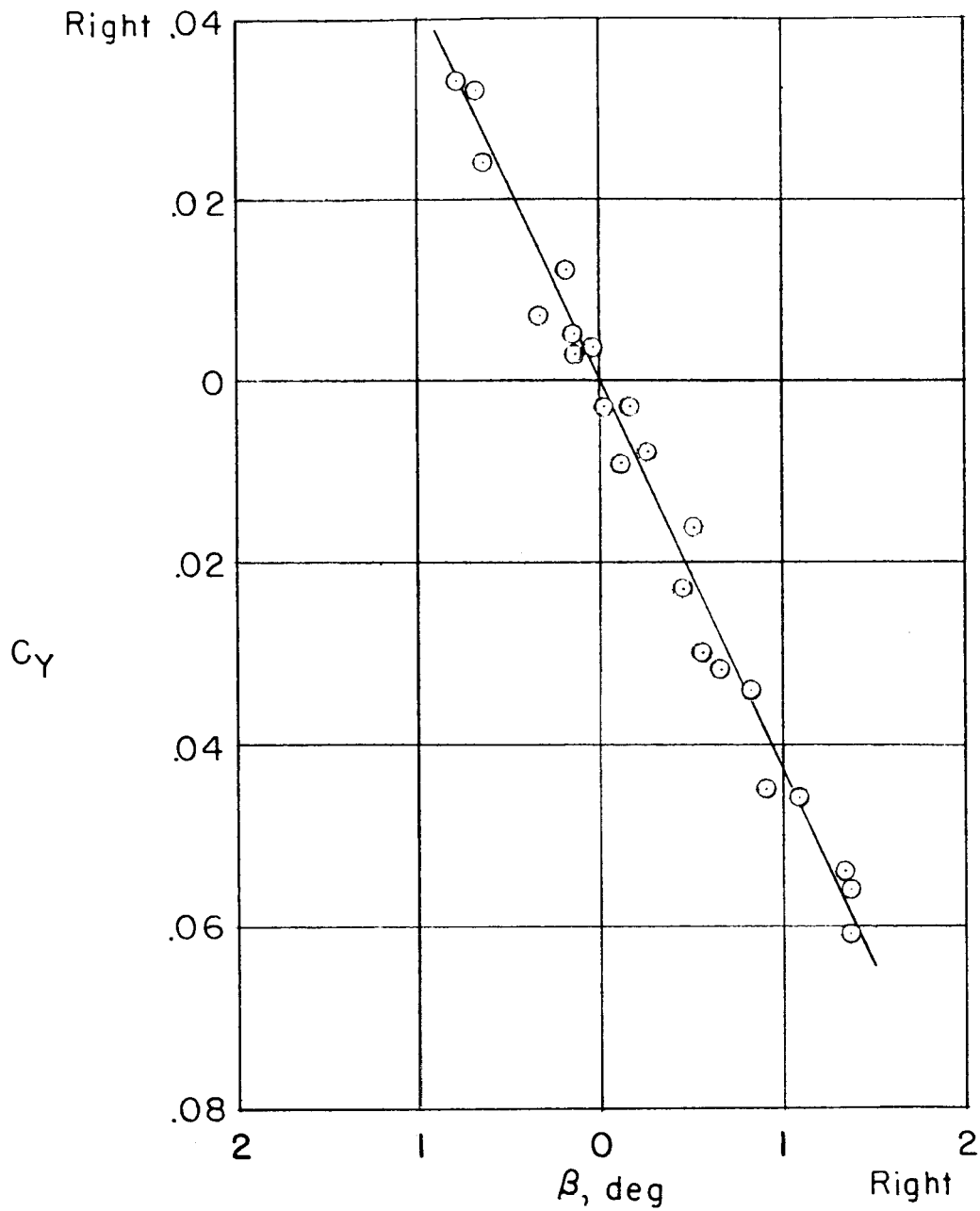


Figure 5.- Vertical-tail-panel lift-curve slope obtained from controls-fixed oscillation of figure 4. Configuration C; $M = 0.89$; $\delta_r \approx 0^\circ$.

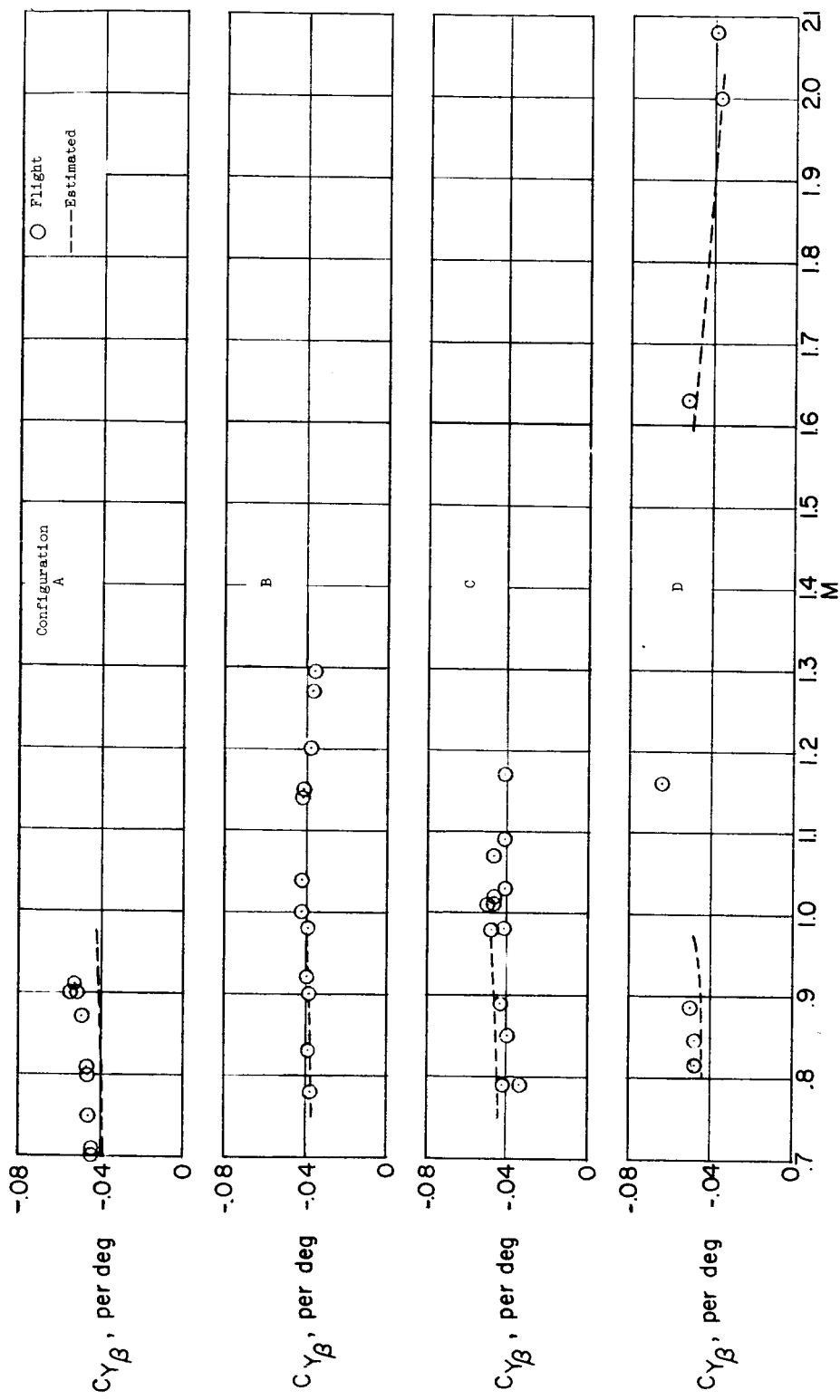


Figure 6.- Effect of sideslip on vertical-tail load. $\delta_T \approx 0^\circ$.

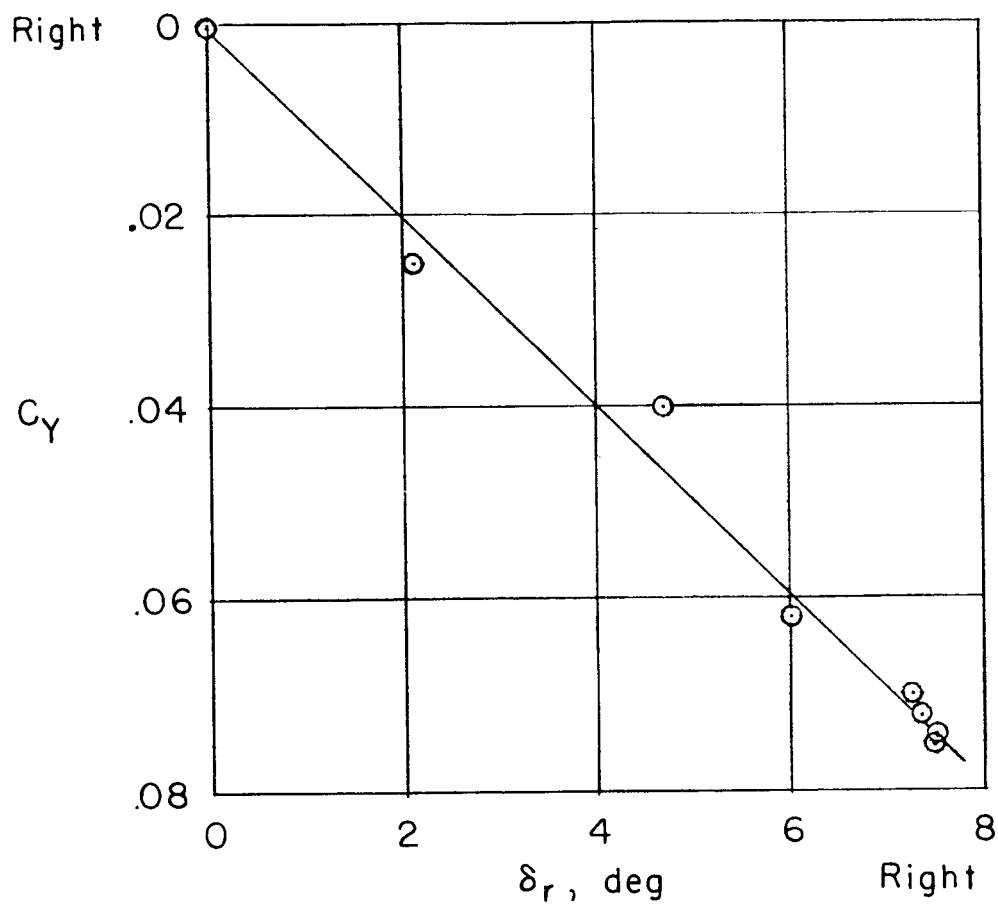


Figure 7.- Contribution of rudder to vertical-tail load obtained from rudder-pulse maneuver of figure 4. Configuration C; $M = 0.89$; $\beta \approx 0^\circ$.

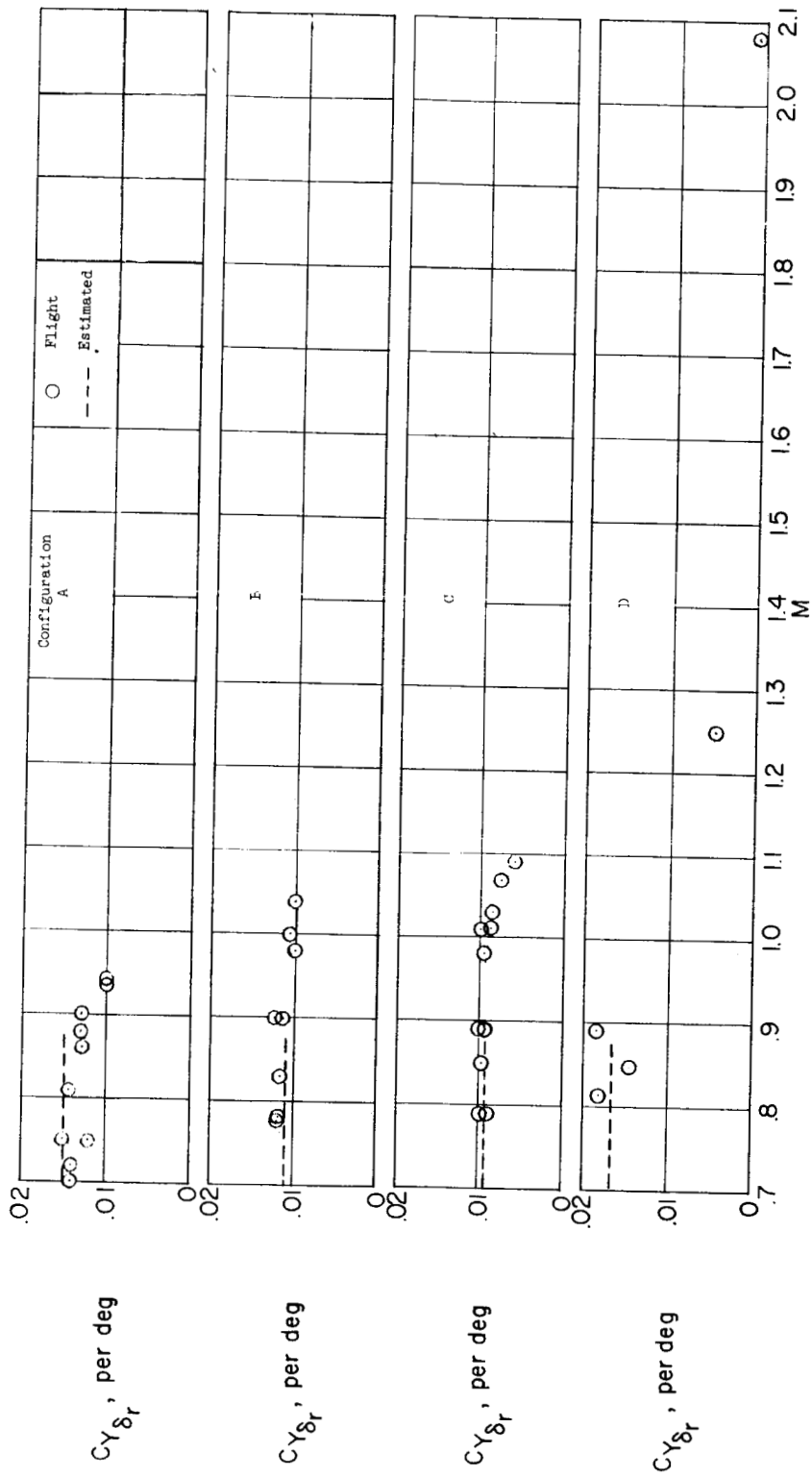


Figure 8.- Effect of rudder on vertical-tail load. $\beta \approx 0^\circ$.

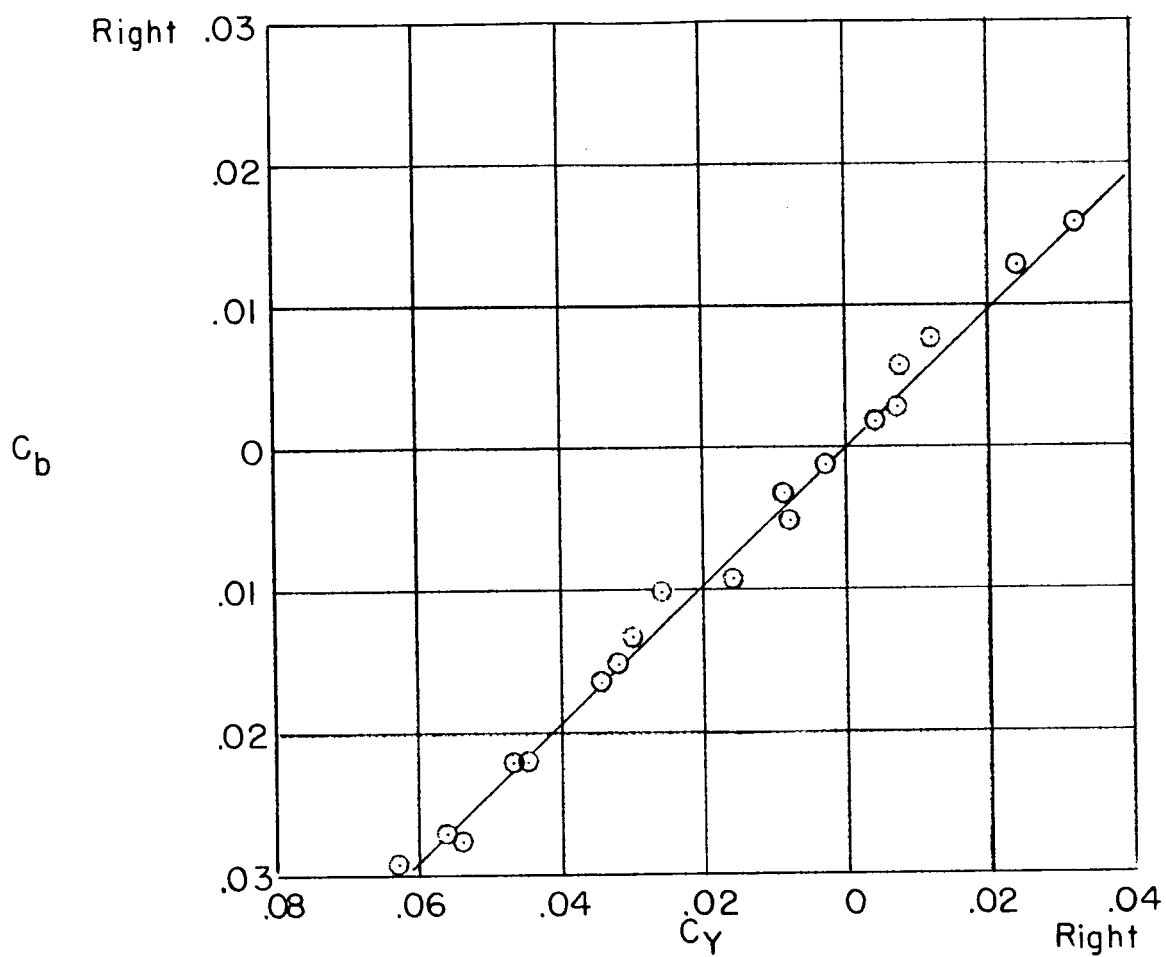


Figure 9.- Variation of bending-moment coefficient with side-force coefficient obtained from controls-fixed oscillation of figure 4. Configuration C; $M = 0.89$; $\delta_r \approx 0^\circ$.

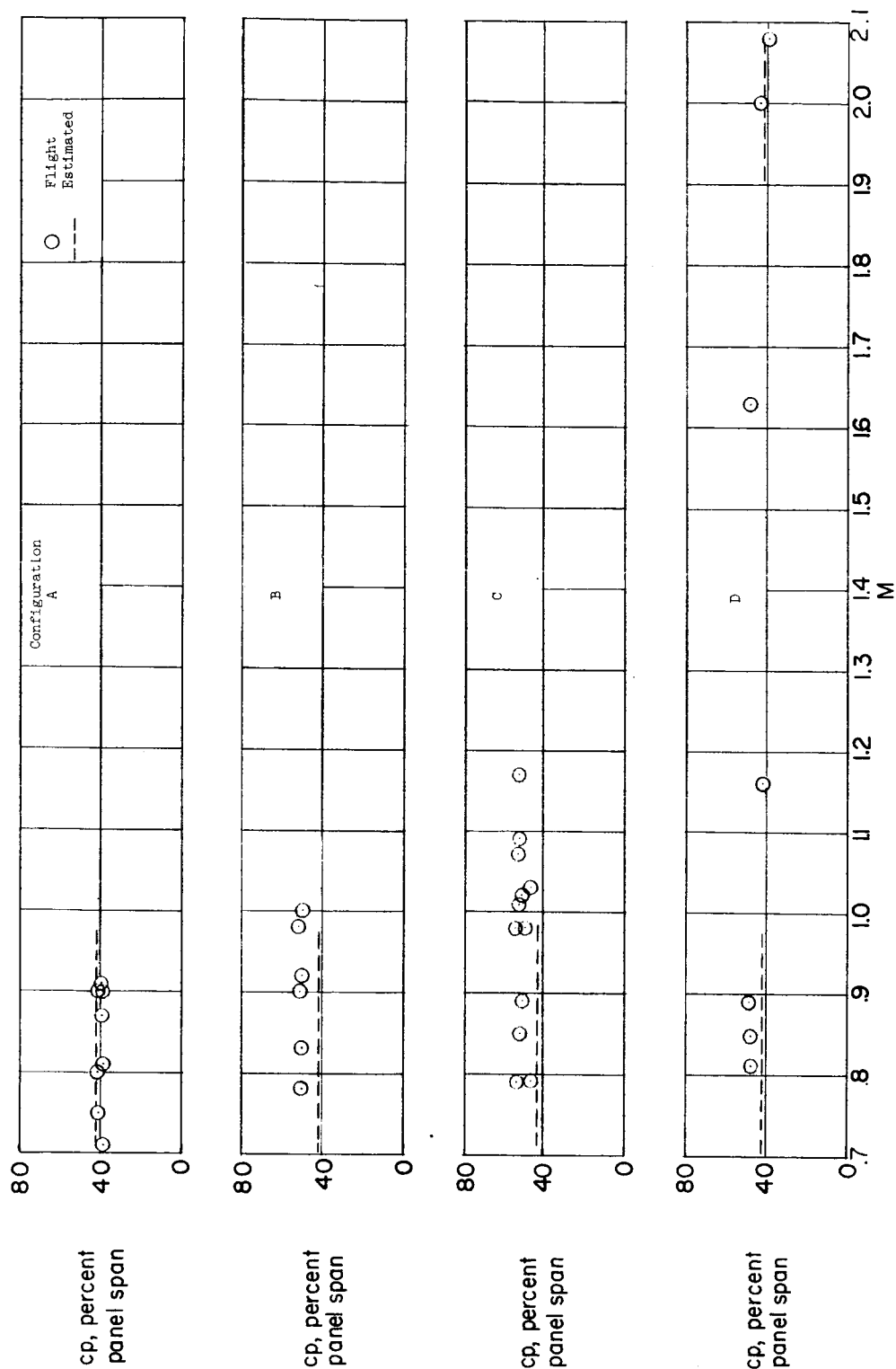


Figure 10.- Spanwise centers of pressure during controls-fixed oscillations.

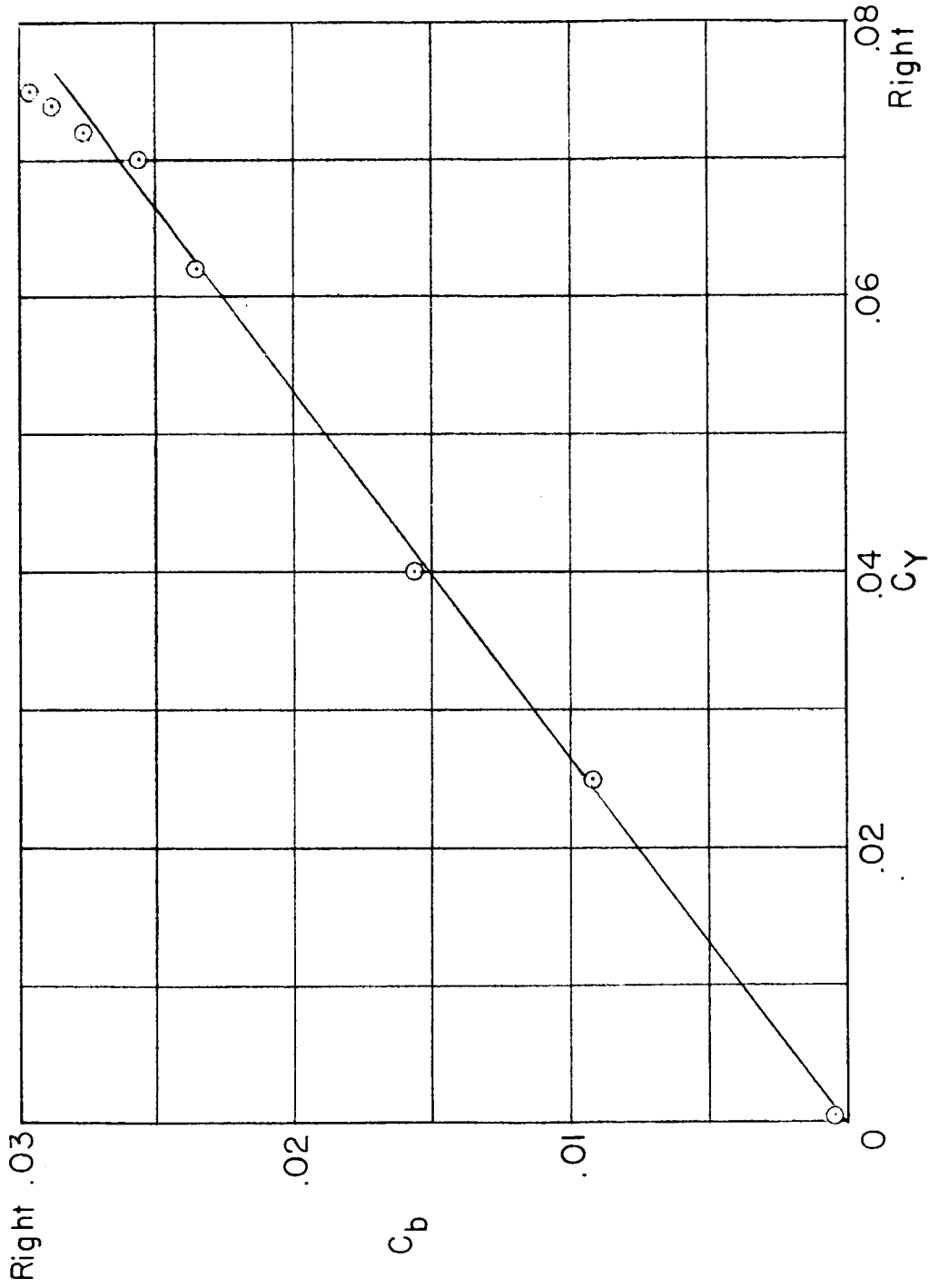


Figure 11.- Variation of bending-moment coefficient with side-force coefficient obtained from rudder-pulse maneuver of figure 4. Configuration C; $M = 0.89$; $\beta \approx 0^\circ$.

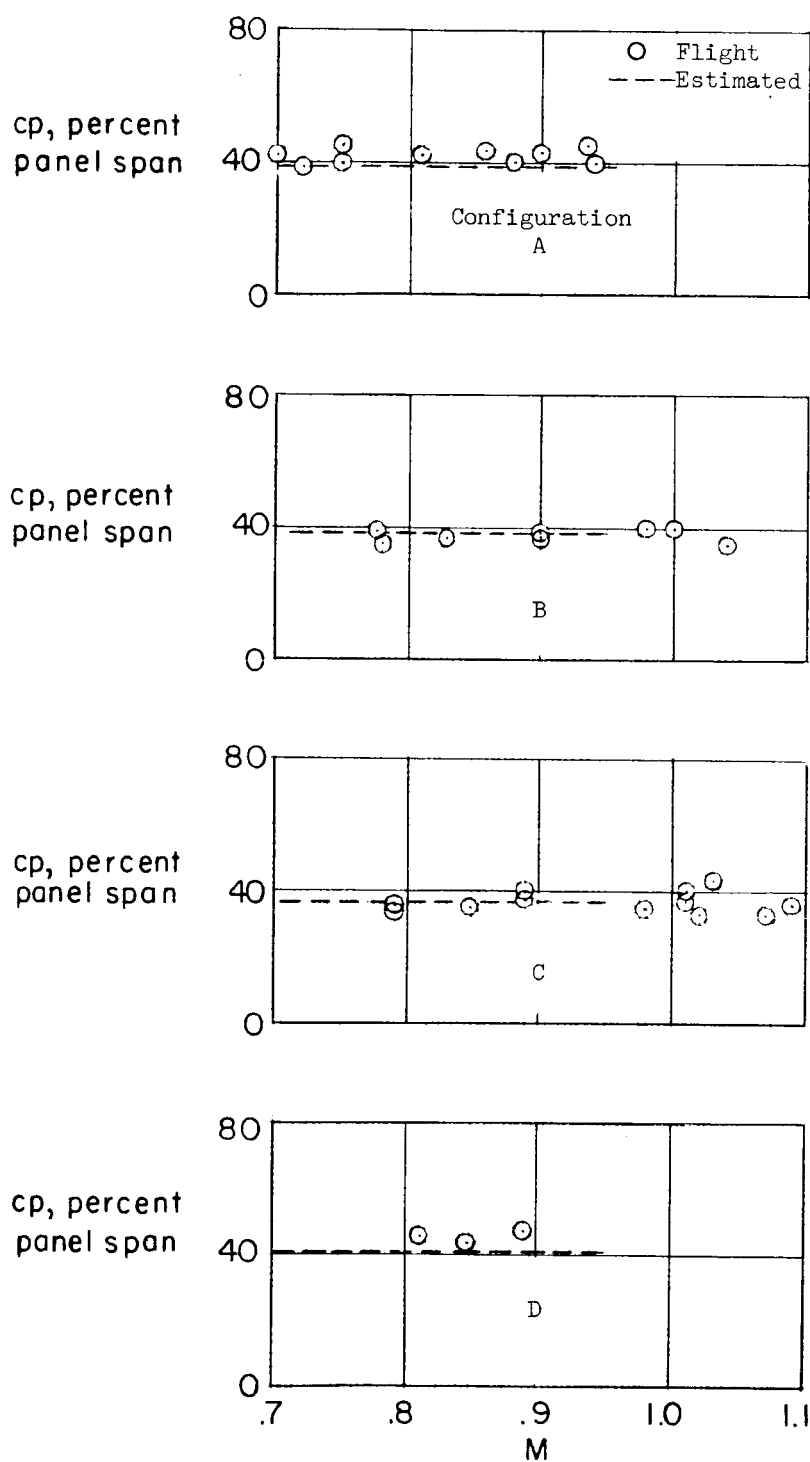


Figure 12.- Spanwise centers of pressure during rudder inputs.

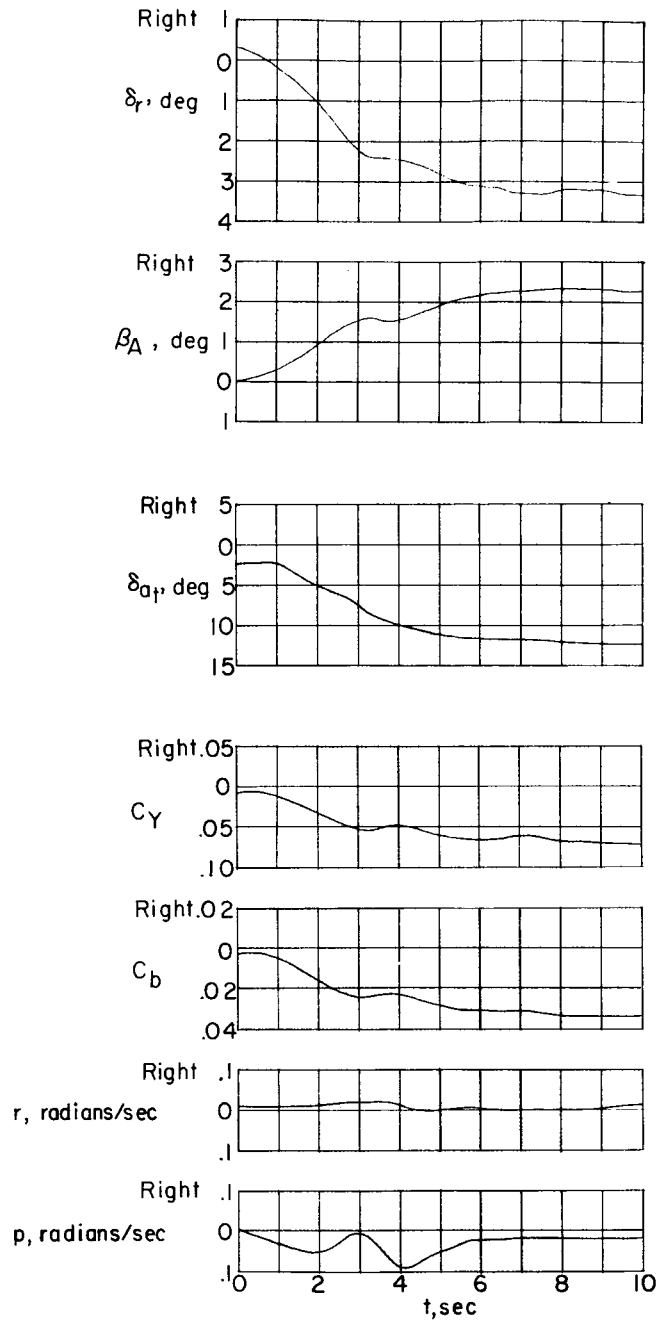


Figure 13.- Time history of a typical steady-sideslip maneuver.
Configuration A; $M = 0.81$.

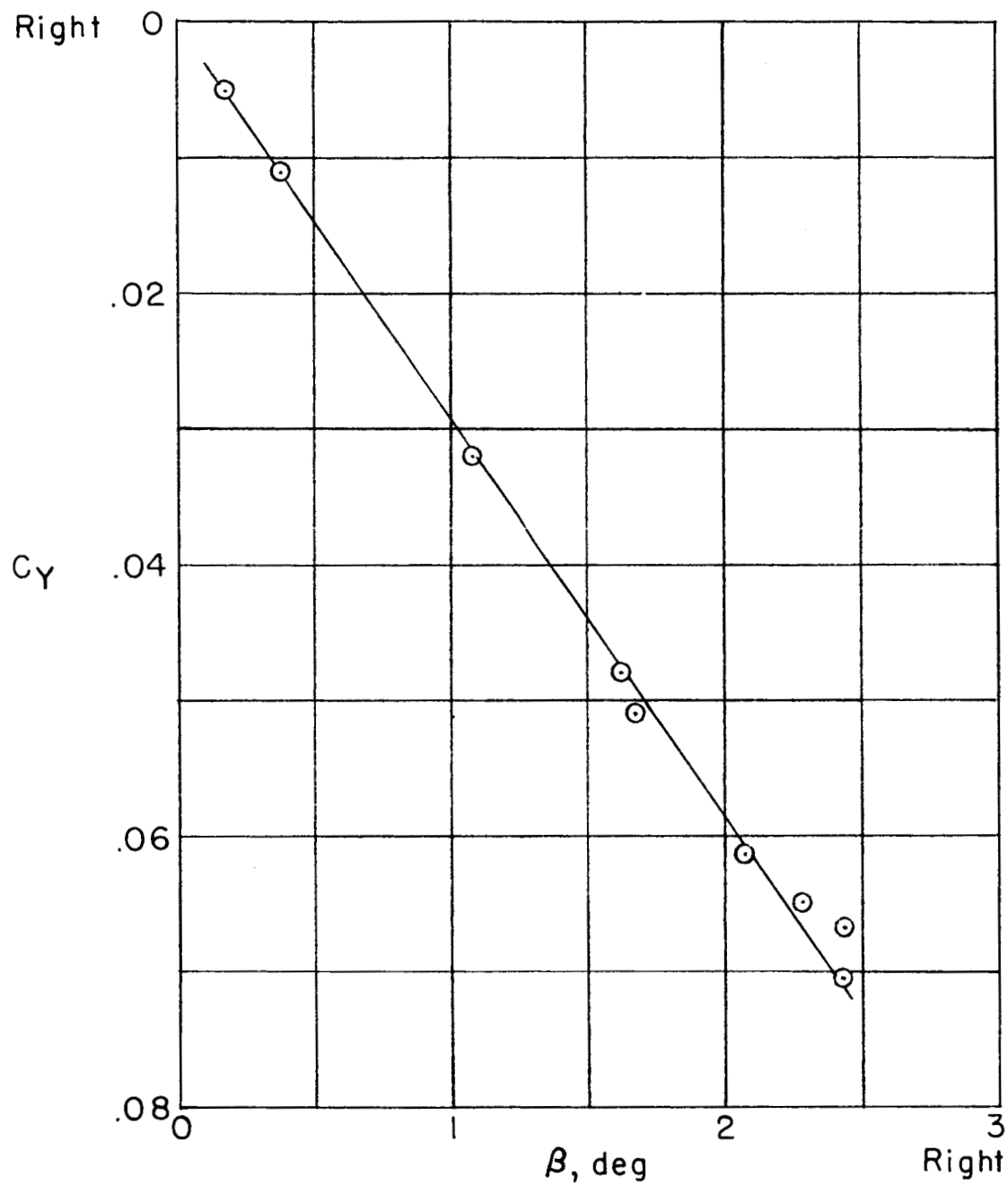


Figure 14.- Variation of side-force coefficient with sideslip obtained during steady-sideslip maneuver of figure 13. Configuration A; $M = 0.81$.

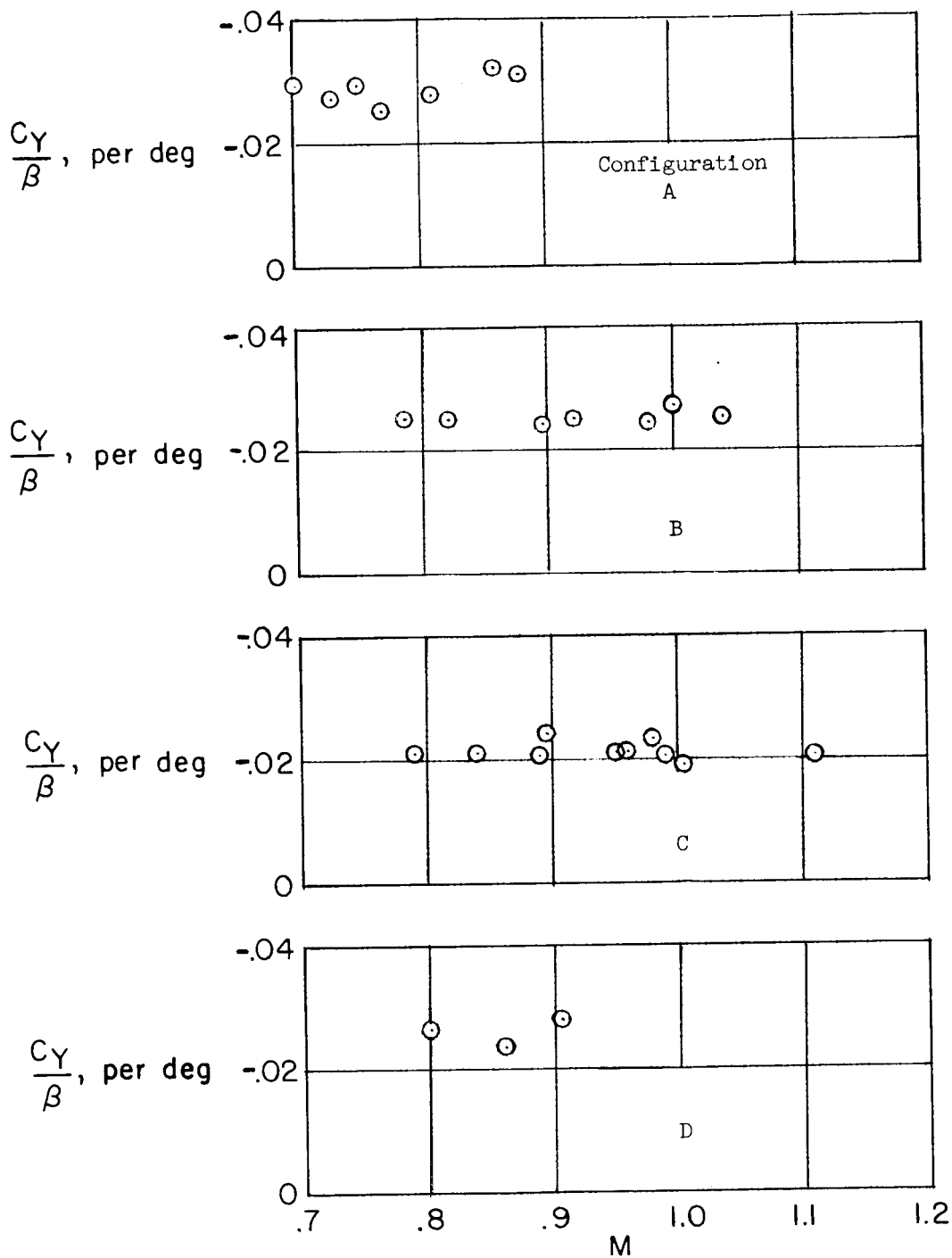


Figure 15.- Slope of variation of side force with sideslip angle during gradually increasing sideslip maneuvers.

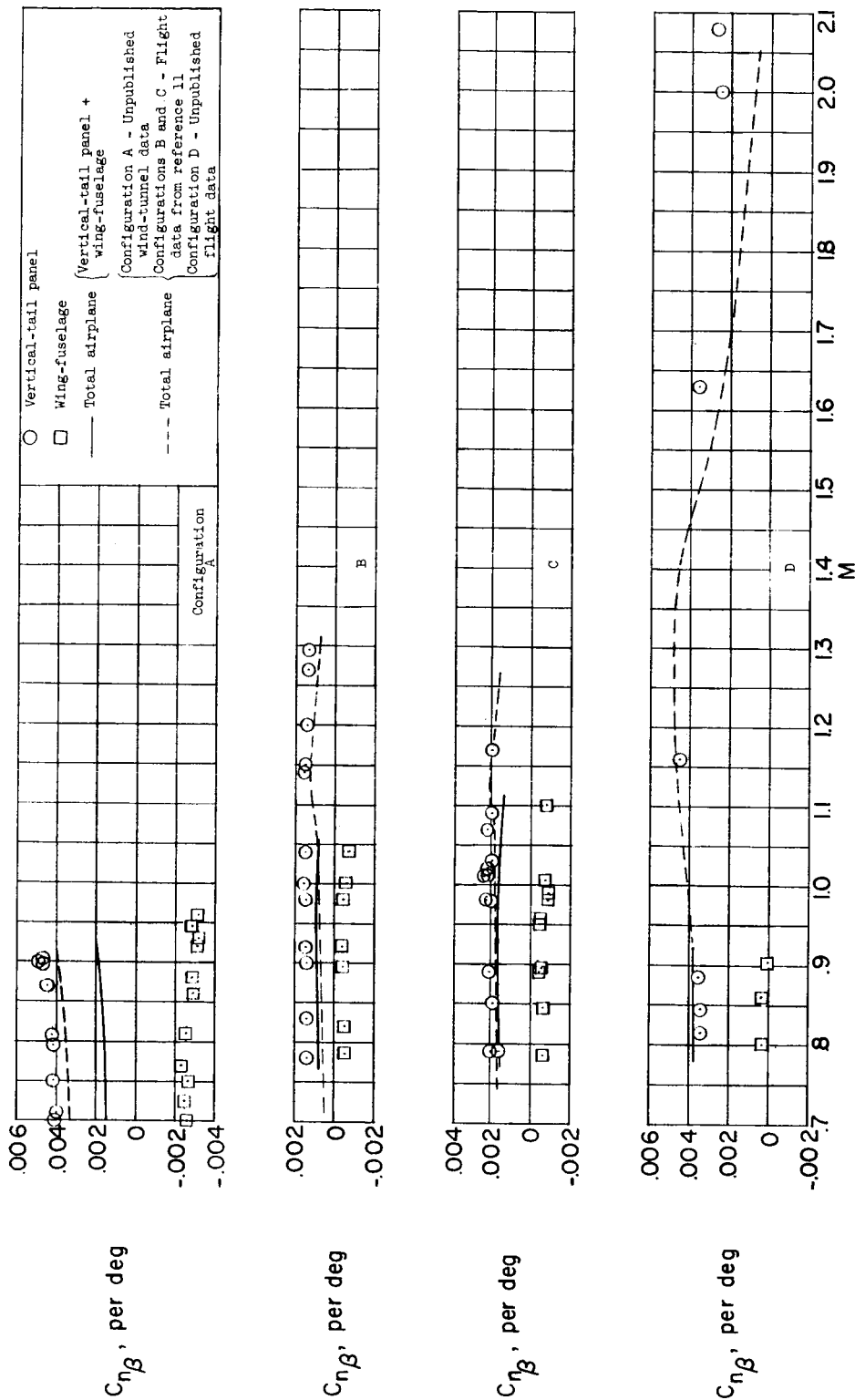


Figure 16.- Component contributions to directional stability.